Analysis of the loop length distribution for the negative weight percolation problem in dimensions $d = 2$ through 6

G. Claussen,* L. Apolo[1,2],† O. Melchert[1],‡ and A. K. Hartmann[1§]
[1] *Institut für Physik, Universität Oldenburg, Carl-von-Ossietzky Strasse, 26111 Oldenburg, Germany*
[2] *City College of the City University of New York, New York, New York 10031, USA*
(Dated: July 13, 2012)

We consider the negative weight percolation (NWP) problem on hypercubic lattice graphs with fully periodic boundary conditions in all relevant dimensions from $d = 2$ to the upper critical dimension $d = 6$. The problem exhibits edge weights drawn from disorder distributions that allow for weights of either sign. We are interested in in the full ensemble of loops with negative weight, i.e. non-trivial (system spanning) loops as well as topologically trivial ("small") loops. The NWP phenomenon refers to the disorder driven proliferation of system spanning loops of total negative weight. While previous studies where focused on the latter loops, we here put under scrutiny the ensemble of small loops. Our aim is to characterize -using this extensive and exhaustive numerical study- the loop length distribution of the small loops right at and below the critical point of the hypercubic setups by means of two independent critical exponents. These can further be related to the results of previous finite-size scaling analyses carried out for the system spanning loops. For the numerical simulations we employed a mapping of the NWP model to a combinatorial optimization problem that can be solved exactly by using sophisticated matching algorithms. This allowed us to study here numerically exact very large systems with high statistics.

PACS numbers:
Keywords:

I. INTRODUCTION

The statistical properties of lattice-path models on graphs, equipped with quenched disorder, have experienced much attention during the last decades. They have proven to be useful in order to characterize, e.g., linear polymers in disordered/random media [1–5], vortex loops in high-T_c superconductivity at zero field [6–9] and the $d = 3$ XY model [10, 11], networks of vortex strings found after a symmetry-breaking phase transition in field theories [12–14], as well as domain wall excitations in disordered media such as spin glasses [15, 16] and the solid-on-solid model [17]. The precise computation of these paths can often be formulated in terms of a combinatorial optimization problem and hence might allow for the application of exact optimization algorithms [18] developed in computer science.

For an analysis of the statistical properties of these lattice path models, geometric observables and scaling concepts similar to those developed in percolation theory [19–21] have been used conveniently. In the past decades, a large number of percolation problems in various contexts have been investigated through numerical simulations. Among those are problems, where the fundamental entities are string-like, similar to the lattice-path models mentioned in the beginning, rather than clusters consisting of occupied nearest neighbor sites as in the case of usual random bond percolation.

In a sequence of recent articles we have introduced [22] and investigated (see below) *the negative-weight percolation* (NWP), a problem with subtle differences as compared to other string-like percolation problems. In the most basic NWP setup, one considers a regular lattice graph with periodic boundary conditions (BCs), where adjacent sites are joined by undirected edges. Weights are assigned to the edges, representing quenched random variables drawn from a distribution that allows for edge weights of either sign. The properties of the weight distribution are further controlled by a tunable disorder parameter, signified ρ. For a given realization of the disorder, one then computes a configuration of loops, i.e. closed paths on the lattice graph, such that the sum of the edge weights that build up the loops is minimal and negative. As an additional optimization constraint we impose the condition that the loops are not allowed to intersect; consequently there is no definition of clusters in the NWP model. Regardless of the spacial dimension of the underlying (hypercubic) lattice graph, the observables are always line-like, i.e. have an intrinsic dimension of $d = 1$. Nevertheless, the loops may be fractal with fractal dimensions $d_f > 1$, see Ref. [23].

The problem of finding these loops numerically can be cast into a minimum-weight path (MWP) problem, outlined in sect. II in more detail. A pivotal observation is that, as a function of the disorder parameter ρ, the NWP model features a disorder driven, geometric phase transition, [22–24] triggered by a vital change of the typical loop size (as discussed below in more detail). In this regard, depending on the precise lattice setup and on the value of ρ, one can identify two different phases: (i) a phase where the loops are "small", meaning that the lin-

*Electronic address: gunnar.claussen@uni-oldenburg.de
†Electronic address: lapolo00@ccny.cuny.edu
‡Electronic address: oliver.melchert@uni-oldenburg.de
§Electronic address: alexander.hartmann@uni-oldenburg.de

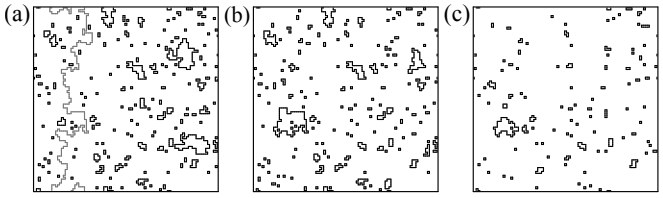

FIG. 1: Samples of minimum weight configurations of loops for a $2D$ square lattice with side length $L=64$ and fully periodic boundary conditions. The snapshots relate to different values of the disorder parameter ρ, where (a) $\rho \approx \rho_c$, (b) $\rho' < \rho_c$, and, (c) $\rho'' < \rho'$. In the limit of large system sizes and above the critical point ρ_c, loops might span the lattice along at least one direction as, e.g., the gray loop in (a). For small values of ρ, loops with a comparatively large length appear to be suppressed exponentially.

ear extensions of the loops are small in comparison to the system size, see Figs. 1(b-c) (therein, the linear extension of a loop refers to its projection onto the independent lattice axes), and, (ii) a phase where "large" loops exist that span the entire lattice, see Fig. 1(a). Regarding these two phases and in the limit of large system sizes, there is a particular value of the disorder parameter, signified as ρ_c, at which system spanning (or "percolating") loops appear for the first time.

Previously, we have investigated the NWP phenomenon for $2D$ lattice graphs [22] using finite-size scaling (FSS) analyses, where we characterized the underlying transition by means of a set of critical exponents. Considering different disorder distributions and lattice geometries, the exponents where found to be universal in $2D$ and clearly distinct from those describing other percolation phenomena. In a subsequent study we investigated the effect of dilution on the critical properties of the $2D$ NWP phenomenon [24]. Therefore we performed FSS analyses to probe critical points along the critical line in the disorder-dilution plane that separates domains that exhibit or do not exhibit system spanning loops. One conclusion of that study was that bond dilution changes the universality class of the NWP problem. Further we found that, for bond-diluted lattices prepared at the percolation threshold of $2D$ random percolation and at full disorder, the geometric properties of the system spanning loops compare well to those of ordinary self-avoiding walks. We performed further simulations for the NWP model on hypercubic lattice graphs in dimensions $d=2$ through 7 [23], where we found evidence for an upper critical dimension $d_u=6$ of the NWP phenomenon. This result was based on monitoring the critical exponents related to the NWP transition (one expects them to stay fixed for $d \geq d_u$). We also studied numerically as well as analytically a variant of the NWP transition on 3-regular random graphs (RRGs), i.e. graphs where each node has exactly 3 neighbors and where there is no regular lattice structure. Hence, we obtained direct access to the mean-field exponents that govern the model for $d \geq d_u$. We obtained excellent agreement between numerical and analytic results and could provide further support for the claim $d_u = 6$.

All of the studies mentioned above where focused on the statistical properties of the largest loop (or more precisely, the *longest* loop) for a given realization of the disorder and the critical properties of the NWP model that derive from an analysis of these loops in the vicinity of the critical point ρ_c. Up to now, limited attention was payed to the ensemble of "small" loops that actually comprise the major part of loop segments in the vicinity of ρ_c. As we found earlier, at this critical point the loops are rather isolated and well separated from each other, resembling a dilute gas of loops (cf. Fig. 1). Further, the normalized and ensemble-averaged probability mass function (pmf) n_ℓ of loops having length ℓ right at ρ_c was studied in Refs. [22, 23]. It exhibits an algebraic decay similar to the distribution of cluster sizes at the critical point in ordinary random percolation [19, 20], i.e.

$$n_\ell(\rho_c) \propto \ell^{-\tau} \quad \text{at} \quad \rho = \rho_c. \tag{1}$$

The numerical values of the decay exponent τ (also termed "Fisher exponent") found for the NWP model in $d = 2$ through 7 are listed in Tab. I. Note that the Fisher exponent is only one out of two independent exponents that characterize the whole ensemble of loops.

In the present article, the second critical exponent that characterizes the ensemble of small loops is addressed. In this regard, the present article discusses the pmf $n_\ell(\rho)$ as function of the disorder parameter ρ. Consequently, the numerical effort to obtain these distributions, in several dimensions $d = 2, \ldots, 6$ was much larger, compared to the previous studies where the distribution was obtained just for $\rho \approx \rho_c$. One of our main results is that for values $\rho < \rho_c$, the pmf appears to scale similar to the distribution of cluster sizes in usual percolation [19, 20], i.e.

$$n_\ell(\rho) \propto \ell^{-\tau} \exp\{-T_{\mathrm{L}}(\rho)\ell\} \quad \text{for} \quad \rho < \rho_c. \tag{2}$$

TABLE I: Critical properties that characterize the NWP phenomenon in $d=2\ldots6$. From left to right: Lattice dimension d, critical point ρ_c, product $\nu_{\mathrm{p}} \cdot d_{f,\mathrm{p}}$ of the critical exponents ν_{p} and $d_{f,\mathrm{p}}$ that describe the divergence of a typical length scale and the fractal dimension $d_{f,\mathrm{p}}$ (measured at ρ_c), respectively, as well as the length fluctuation exponent γ_{p}. Further, the table lists the Fisher exponent τ and the loop-length cutoff exponent σ. Note that the figures in all but the two right columns are taken from Ref. [23]. The last column is meant to check the scaling relation $\gamma_{\mathrm{p}} = (3-\tau)/\sigma$. The additional subscript p indicates that these exponents result from an analysis of the percolating loops.

d	L	ρ_c	$\nu_{\mathrm{p}} d_{f,\mathrm{p}}$	γ_{p}	τ	σ	$(3-\tau)/\sigma$
2	512	0.340(1)	0.53(3)	0.77(7)	2.59(3)	0.53(3)	0.77(10)
3	64	0.1273(3)	0.69(2)	-0.09(3)	3.07(1)	0.71(1)	-0.10(1)
4	21	0.0640(2)	0.78(3)	-0.66(5)	3.55(2)	0.78(2)	-0.71(1)
5	12	0.0385(2)	0.86(4)	-1.06(7)	3.86(3)	0.88(2)	-0.98(1)
6	6	0.0265(2)	1.00(3)	-0.99(3)	4.00(2)	0.97(4)	-1.03(2)

Therein, the exponential factor accounts for the observation that below the critical point ρ_c the proliferation of "long" (still non-spanning) loops is suppressed due to some finite "loop size cut-off parameter". The latter might be captured by means of a scaling parameter $T_{\rm L}(\rho)$ [13] which depends on the subtleties of the disorder. Its inverse $\ell_0(\rho) = 1/T_{\rm L}(\rho)$ relates to a typical length scale to which the perimeter of the loops is limited at a given value of ρ and it should not depend on the side length L of the system (at least in the limit of large system sizes where a loop of, say, length ℓ_0 fits well into the simulation box). Therefore, loop configurations a[19, 20] small values of ρ are consistent with a spanning probability $P_L(\rho < \rho_c) \to 0$ in the limit of large system sizes ($L \to \infty$). As the critical point is approached from below the loop size cut-off parameter vanishes, giving rise to the purely algebraic decay of n_ℓ observed at ρ_c, as in Eq. (1), featuring loops with length ℓ on virtually all length scales. (A qualitatively similar observation in the context of high-T_c superconductors is referred to as "Onsager vortex-loop unbinding" that signals the superconductor to normal metal transition [6, 7]. Further, in string theory, the analog observation is referred to as "Hagedorn transition" [12, 13].) The decrease of the parameter $T_{\rm L}(\rho)$ can be related to a second, independent exponent that, in addition to τ, serves to characterize the ensemble of small loops. The respective critical exponent σ is defined via

$$T_{\rm L}(\rho) \propto |\rho - \rho_c|^{1/\sigma} \ , \tag{3}$$

where σ might be referred to as "loop-size cut-off" exponent (i.e. the critical exponent related to the loop-size cut-off parameter $T_{\rm L}$) and where ρ approaches ρ_c from below. Similarly, the corresponding lengthscale ℓ_0, to which the loops are confined, diverges. This implies that loops might get arbitrarily long, limited only by the finite size of the underlying lattice. One might expect a maximal loop length of $\ell_{\max} \sim L^{d_f}$, where d_f denotes the fractal scaling dimension of the loops. Thus, at ρ_c and in the limit $L \to \infty$, the distribution of the loop perimeter exhibits an algebraic decay, solely governed by the fisher exponent τ. Finally, according to scaling theory [19, 20], the scaling relations

$$\nu_{\rm p} d_{f,{\rm p}} = 1/\sigma, \tag{4a}$$
$$\gamma_{\rm p} = (3-\tau)/\sigma \tag{4b}$$

should hold, relating σ (as measured for the small loops) to $\nu_{\rm p}$, $d_{f,{\rm p}}$ and $\gamma_{\rm p}$ (all measured from the system spanning loops; indicated by the subscript p). These three exponents signify the critical exponents that describe the divergence of the correlation length, the scaling dimension of the loops, and the fluctuations of the loop order-parameter, respectively.

The remainder of the present article is organized as follows. In section II, we introduce the model in more detail and we outline the algorithm used compute the loop configurations. In section III, we list the results of our numerical simulations and in section IV we conclude with a summary. Note that an extensive summary of this paper is available at the *papercore database* [25].

II. MODEL AND ALGORITHM

In the present article we consider hypercubic lattice graphs $G = (V, E)$ with side length L and fully periodic boundary conditions (BCs) for all relevant dimensions $d = 2$ through 6. The considered graphs have $N = |V| = L^d$ sites $i \in V$ and a number of $|E| = zN/2$ undirected edges $\{i, j\} \in E$ that join adjacent sites $i, j \in V$. Above, z signifies the coordination number of the lattice geometry, where $z = 2d$. We further assign a weight ω_{ij} to each $\{i, j\} \in E$. These weights represent quenched random variables that introduce disorder to the lattice. Here we consider independent identically distributed weights which either have just weight one (probability 1-ρ) or are drawn (probability ρ) from a Gaussian distribution with zeor mean and veriance one. Hence, the disorder distribution is given by

$$P(\omega) = \rho \exp\left(-\omega^2/2\right)/\sqrt{2\pi} + (1-\rho)\delta(\omega - 1), \tag{5}$$

that explicitly allows for loops $\mathcal{L}$ with a negative total weight $\omega_{\mathcal{L}} = \sum_{\{i,j\}\in\mathcal{L}} \omega_{ij}$. To support intuition: For any nonzero value of the disorder parameter ρ, a sufficiently large lattice will exhibit at least "small" loops that exhibit a negative weight, see Fig. 1(c). If the disorder parameter is large enough, system spanning loops with negative weight will exist, see Figs. 1(a).

The NWP problem then reads as follows: Given a realization of the disorder for a hypercubic lattice graph G, determine a set $\mathcal{C}$ of loops such that the configuration energy, defined as the sum of all the loop-weights $\mathcal{E} = \sum_{\mathcal{L}\in\mathcal{C}} \omega_{\mathcal{L}}$, is minimized. As further optimization constraint, the loops are not allowed to intersect. Note that due to the "energy minimization principle" of the optimization procedure, the weight of an individual loop is necessarily smaller than zero. The configuration energy $\mathcal{E}$ is the quantity subject to optimization and the result of the optimization procedure is a set of loops $\mathcal{C}$, obtained using an appropriate transformation of the original graph [26]. For the transformed graphs, *minimum-weight perfect matchings* (MWPMs) [27–29] are calculated, that serve to identify the loops for a given realization of the disorder. Since exact MWPMs can be obtained in polynomial time, this procedure allows for an efficient implementation [30] of the simulation algorithms. Here, we give a brief description of the algorithmic procedure that yields a minimum-weight set of loops for a given realization of the disorder. Fig. 2 illustrates the three basic steps, detailed below:

(1) each edge, joining adjacent sites on the original graph G, is replaced by a path of 3 edges. Therefore, 2 "additional" sites have to be introduced for each edge in E. Therein, one of the two edges connecting an additional site to an original site gets the same weight as

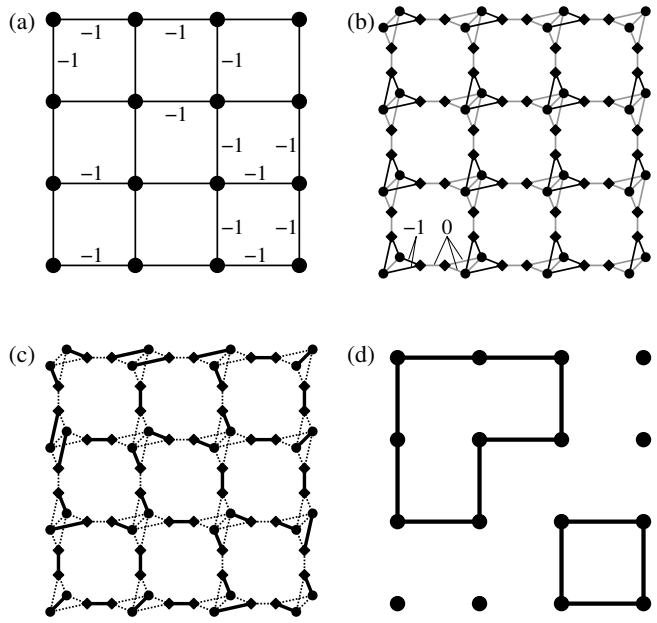

FIG. 2: Illustration of the algorithmic procedure: (a) original lattice G with edge weights. For clarity, a bimodal distribution that yields edge-weights ± 1 is considered. Further, only negative edge-weights are shown. Unlabeled edges have weight $+1$. (b) auxiliary graph G_{A} with proper weight assignment. Black edges carry the same weight as the respective edge in the original graph and gray edges carry zero weight, (c) minimum-weight perfect matching (MWPM) M: bold edges are matched and dashed edges are unmatched, and (d) loop configuration (bold edges) that corresponds to the MWPM depicted in (c).

the corresponding edge in G. The remaining two edges get zero weight. The original sites $i \in V$ are then "duplicated", i.e. $i \to i_1, i_2$, along with all their incident edges and the corresponding weights. For each of these pairs of duplicated sites, one additional edge $\{i_1, i_2\}$ with zero weight is added that connects the two sites i_1 and i_2. The resulting auxiliary graph $G_{\mathrm{A}} = (V_{\mathrm{A}}, E_{\mathrm{A}})$ is shown in Fig. 2(b), where additional sites appear as squares and duplicated sites as circles. Fig. 2(b) also illustrates the weight assignment on the transformed graph G_{A}. Note that while the original graph (Fig. 2(a)) is symmetric, the transformed graph (Fig. 2(b)) is not. This is due to the details of the mapping procedure and the particular weight assignment we have chosen. A more extensive description of the mapping can be found in [16].

(2) a MWPM on the auxiliary graph is determined via exact combinatorial optimization algorithms [31]. A MWPM is a minimum-weighted subset M of E_{A}, such that each site contained in V_{A} is met by precisely one edge in M. This is illustrated in Fig. 2(c), where the solid edges represent M for the given weight assignment. The dashed edges are not matched. Due to construction, the auxiliary graph consists of an even number of sites and the transformation procedure described in step (1) guarantees that a perfect matching exists. Note that a MWPM can be computed in polynomial time as a function of the number of sites, hence large systems with hundreds of thousands of sites are feasible.

(3) finally it is possible to find a relation between the matched edges M on G_{A} and a configuration of negative-weighted loops $\mathcal{C}$ on G by tracing back the steps of the transformation (1). As regards this, note that each edge contained in M that connects an additional site (square) to a duplicated site (circle) corresponds to an edge on G that is part of a loop, see Fig. 2(d). Note that, by construction of the auxiliary graph, for each site i_1 or i_2 matched in this way, the corresponding "twin" site i_2/i_1 must be matched to an additional site as well. This guarantees that wherever a path "enters" a site of the original graph, the paths also "leaves" the site, corresponding to the defining condition of loops. All the edges in M that connect like sites (i.e. duplicated-duplicated, or additional-additional) carry zero weight and do not contribute to a loop on G. Once all loop segments are found, a depth-first search [26, 28] can be used to identify the loop set $\mathcal{C}$ and to determine the geometric properties of the individual loops. Here, the exemplary weight assignment illustrated in Fig. 2(a) yields 2 loops, i.e. $\mathcal{C} = \{\mathcal{L}_1, \mathcal{L}_2\}$, with weights $\omega_{\mathcal{L}_1} = \omega_{\mathcal{L}_2} = -4$ and lengths $\ell_1 = \sum_{\{i,j\}\in\mathcal{L}_1} 1 = 8$, $\ell_2 = 4$. Hence, the configurational energy reads $\mathcal{E} = -8$.

The result of the calculation is a collection $\mathcal{C}$ of loops such that the total loop weight, and consequently the configuration energy $\mathcal{E}$, is minimized. Hence, one obtains a global collective optimum of the system. Obviously, all loops that contribute to $\mathcal{C}$ possess a negative weight. Also note that the choice of the weight assignment in step (1) is not unique, i.e. there are different possibilities to choose a weight assignment that all result in equivalent sets of matched edges on the transformed lattice, corresponding to the minimum-weight collection of loops on the original lattice. Some of these weight assignments result in a more symmetric transformed graph, see e.g. [26]. However, this is only a technical issue that does not affect the resulting loop configuration. Finally, for the purpose of illustration, a small $2D$ lattice graph with free BCs was chosen intentionally. The algorithmic procedure extends to higher dimensions and fully periodic BCs in a straight-forward manner.

In the remainder of the article, we will use the procedure outlined above in order to study the pmf of loop lengths in the NWP model on hypercubic lattice graphs in $d = 2$ through 6.

III. RESULTS

Within our extensive numerical studies, we performed exact NWP loop calculations for dimensions $d = 2$ through 6 for various values $\rho \leq \rho_c$ while averaging over many realizations of the disorder. Details are given in Tab. II.

In order to get a grip on the loop-size cut-off parameter

σ for a particular hypercubic lattice setup of dimension d, the pmf $n_\ell(\rho)$ of the loop length needs to be obtained for different values of the disorder parameter $\rho \leq \rho_c$. Then, a best fit to the form $n_\ell(\rho) = n_0 \ell^{-\tau} \exp\{-T_{\rm L}(\rho)\ell\}$ might be used to obtain the three fit parameters n_0, τ, and $T_{\rm L}(\rho)$ for different values of ρ. Finally, the sequence of fit parameters $T_{\rm L}(\rho)$ might be analyzed to yield the exponent σ according to Eq. (3).

However, a different procedure appears to be more appealing: from previous simulations in dimensions $d = 2$ through 7, reported in Refs. [22, 23], we found that the pmf $n_\ell(\rho_c)$ exhibits an algebraic decay governed by the exponent τ. For the largest lattice graphs simulated for the various dimensions d, we obtain the numerical estimates listed in Tab. I. For the corresponding data analyses, very small loops have to be neglected since they are affected by the granularity of the lattice and very large loops have to be withdrawn since they are affected by the lattice boundaries. Once the exponent τ for a given dimension d is obtained, it can be utilized in the analysis of the loop length pmf at $\rho < \rho_c$ to limit the number of fit parameters to only two (i.e. n_0 and $T_{\rm L}$), allowing for a more precise estimate of the individual values of $T_{\rm L}(\rho)$.

So as to get a grip on the loop size cut-off parameter σ, the loop perimeter distribution was obtained for different values of the disorder parameter $\rho \leq \rho_c$ and the data was fitted using a function as given in Eq. (2), with an additional normalization factor. E.g., in $d = 2$ we use $\tau = 2.59$ fixed, see Tab. I and Fig. 3, wherein the fit intervals for individual values of ρ where restricted to the range $[\ell_{\rm min}, \ell_{\rm max}]$. We further fixed $\ell_{\rm min} = 10$ and $\ell_{\rm max} = 60$ at $\rho = 0.24$ (the upper bound shifting up to $\ell_{\rm max} = 150$ at ρ_c). The resulting values for the cut-off parameter were then analyzed using a three parameter fit to functions of the form of Eq. (3), i.e. $T_{\rm L}(\rho) = A|\rho - \rho_c^{\rm eff}|^{1/\sigma}$. Therein the amplitudes A are not of interest and the effective critical points $\rho_c^{\rm eff}$ can be expected to differ slightly from the asymptotic critical points listed in Tab. I (see discussion below). The resulting loop-length cut-off parameters σ are also listed in Tab. I.

For $d = 2$ systems of side length $L = 512$ the analysis yields $\sigma = 0.53(3)$ and $\rho_c^{\rm eff} = 0.344(2)$, see Fig. 4 (at $L = 256$ we find $\rho_c^{\rm eff} = 0.346(2)$ and $\sigma = 0.53(2)$). For all values of ρ considered, the data curves of $T_{\rm L}$ at

TABLE II: Simulation parameters: we performed our study for n_ρ values of the disorder parameter ρ in intervals $[\rho_1, \rho_2]$ and for a number n_R of realizations, for the different dimensions d and system sizes L.

d	L	$[\rho_1, \rho_2]$	n_ρ	n_R
2	256	[0.24, 0.34]	11	$\sim 2\times10^4$
2	512	[0.24, 0.34]	16	6400
3	64	[0.075, 0.1245]	100	4800
4	21	[0.022, 0.058]	19	8000
5	12	[0.02, 0.038]	19	6400
6	6	[0.015, 0.025]	21	$\sim 5\times10^4$

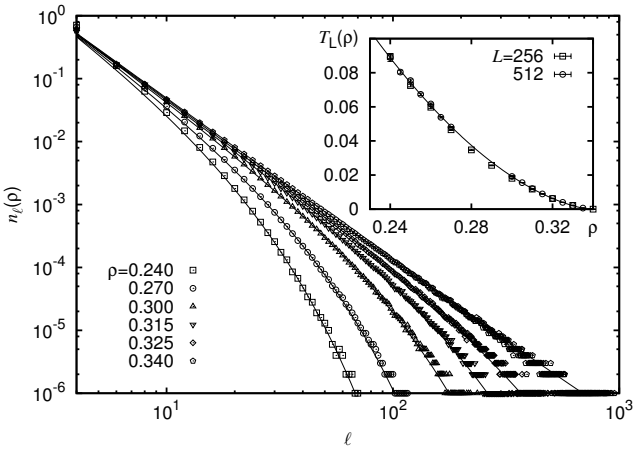

FIG. 3: Results for $d = 2$ square lattice graphs. The main plot shows the probability mass functions $n_\ell(\rho)$ of the loop perimeter ℓ for different values of the disorder parameter ρ for square systems of side length $L = 512$. The data curves illustrate the suppression of loops with a perimeter larger than some cut-off length scale ℓ_0, related to a finite "loop size cut-off parameter" $T_{\rm L}(\rho)$ for $\rho < \rho_c$ (see text). The data curves fit well to functions of the form of Eq. (2). Right at ρ_c the data curve exhibits a pure algebraic decay according to Eq. (1). The inset compares the resulting values of the cut-off parameter $T_{\rm L}(\rho)$ for systems of side length $L = 512$ and $L = 256$, where the solid line indicates a best fit to the $L = 512$ data using a function with four free parameters as explained in the text.

$L = 256$ and $L = 512$ compare well as shown in the inset of Fig. 3. This finding is further consistent with the usual scaling relation $1/(\nu_{\rm p} d_{f,{\rm p}}) = \sigma$ that relates σ to $\nu_{\rm p}$ and $d_{f,{\rm p}}$, where the latter two exponents signify the critical exponent that describes the divergence of the correlation length and the scaling dimension of the loops at the critical point, respectively. From the respective values previously obtained [22] one readily finds $1/(\nu_{\rm p} d_{f,{\rm p}}) = 0.53(3)$. Only the location of the (effective) critical point $\rho_c^{\rm eff} = 0.344(2)$, as estimated from the complete ensemble of loops at the particular system size $L = 512$, differs slightly from the one obtained from the scaling analysis of the percolating loops, i.e. $\rho_c = 0.340(1)$ [22] (a similar effect was found in the analysis of a $d = 3$ vortex loop network in Ref. [10]). Bearing in mind that the latter value represents an extrapolation to the thermodynamic limit, the aforementioned difference is likely due to finite-size effects. In this regard it does not come as a surprise that an analysis of the loop size cut-off parameter according to Eq. (3) for fixed $\rho_c^{\rm eff} = 0.340$ (instead of $\rho_c^{\rm eff} = 0.344$) yields the exponent $\sigma = 0.61(1)$ which significantly overestimates the result obtained from the three parameter fit reported above. Finally, a four parameter fit according to $T_{\rm L}(\rho) = T_{\rm L}' + A|\rho - \rho_c^{\rm eff}|^{1/\sigma}$ at $L = 512$ (see inset of Fig. 3) results in the estimates $T_{\rm L}' = 0.001(1)$, $\rho_c^{\rm eff} = 0.348(6)$ and $\sigma = 0.55(3)$, with the latter two fit parameters in agreement with the ones found above and $T_{\rm L}'$ in agree-

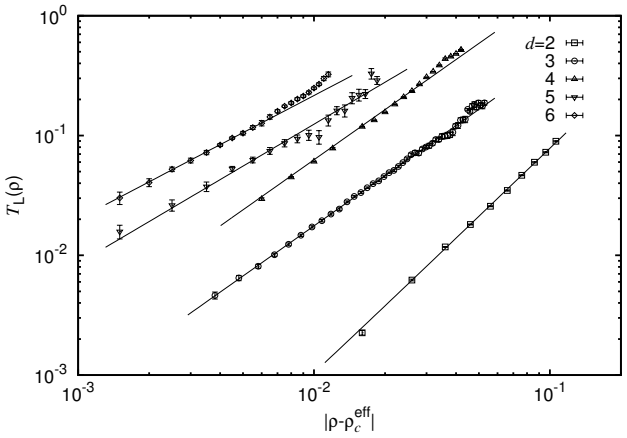

FIG. 4: Scaling analysis of the loop size cut-off parameter $T_{\rm L}(\rho)$ in dimensions $d = 2$ through 6. The solid lines indicate fits to functions of the form $T_{\rm L}(\rho) = A|\rho - \rho_c^{\rm eff}|^{1/\sigma}$. Therein the amplitudes A are not of interest and the effective critical points $\rho_c^{\rm eff}$ can be expected to differ slightly, but within statistical error bars, from the asymptotic critical points listed in Tab. I. The resulting loop-length cut-off parameters σ are also listed in Tab. I.

ment with zero as one would naively expect.

So as to facilitate a qualitative comparison, considering $d = 3$ hypercubic lattices with $L = 64$ we obtained the effective critical point $\rho_c^{\rm eff} = 0.1278(1)$ which slightly overestimates the asymptotic value of $\rho_c = 0.1273(3)$ (similar to what we observed above in $2D$), see Fig. 4. The scaling exponent $\sigma = 0.71(1)$ compares well to the product $\nu_{\rm p} \cdot d_{f,{\rm p}} = 0.69(2)$ for the respective dimension. In the analysis of the data for $d > 3$ we obtained most satisfactory fits by fixing the parameters $\rho_c^{\rm eff}$ to their expected asymptotic values ρ_c listed in Tab. I. The analysis of the loop size cut-off parameter in dimensions $d = 2$ through 6 are shown in Fig. 4 and summarized in Tab. I.

In higher dimensions we also checked that the loop size cut-off parameter $T_{\rm L}(\rho)$ at a given value of ρ is practically independent of the system size (however, for larger system sizes the loop yield is bigger and hence the statistics get more reliable). E.g., for $d = 4$ hypercubic lattices at $\rho = 0.026$, i.e. with some distance to the critical point $\rho_c = 0.0640(2)$, we obtained $T_{\rm L}(0.026) = 0.43(5)$ at $L = 16$ and $T_{\rm L}(0.026) = 0.45(4)$ at $L = 21$. Close to the critical point at $\rho = 0.058$ we further find $T_{\rm L}(0.058) = 0.35(1)$ at $L = 16$ and $T_{\rm L}(0.058) = 0.036(1)$ at $L = 21$. Further, we observe that in any dimension considered, the scaling relation $\gamma_{\rm p} = (3 - \tau)/\sigma$ appears to be satisfied within errorbars.

IV. CONCLUSIONS

In the presented analysis of the NWP model, we performed numerical simulations on hypercubic lattice graphs for all dimensions relevant for the model, i.e. d=2 through 6. The aim of the study was to characterize the ensemble of small loops in the NWP model using two independent critical exponents: the Fisher exponent τ (which was already known from previous studies, see Ref. [23]), and the loop-length cut-off exponent σ. Both exponents can be determined by means of an analysis of the probability mass function $n_\ell(\rho)$ measuring the distribution of loop lengths ℓ, considering a sequence of different values ρ close to but below the critical point. This implies a huge numerical effort, since we had to study in different dimensions large systems, for several values of the disorder parameter, while averaging over many realizations of the disorder. For the numerical simulations we used a mapping of the NWP model to a combinatorial optimization problem that allows to obtain configurations of minimum weight loops via exact algorithms. Note that due to the small side lengths of the lattice graphs that are accessible in high dimensions, the data analysis is notoriously difficult at large values of d. However, we find the results regarding the exponent σ consistent with the scaling relations Eqs. (4a) and (4b) for any dimension considered (see Tab. I). Thus, via this extensive numerical study we have completed a comprehensive description of the static behavior of the NWP model in all relevant dimensions $d = 2, \ldots, 6$.

In particular, many of the $d = 3$ loop models studied in the literature report on values for the critical exponents τ and σ that are close to $\tau = 3.07(1)$ and $\sigma = 0.71(1)$ ($1/\sigma = 1.41(2)$) found here. E.g., Ref. [7] obtains $\tau = 2.4(1)$ (however, in a previous study they report $\tau = 3$, see Ref. [6]) and $1/\sigma = 1.45(5)$ (in that study the latter quantity was called γ) for the $d = 3$ uniformly frustrated XY model as well as for the lattice Ginzburg-Landau model in a frozen gauge approximation, and Ref. [8] yields $\tau = 2.8(1)$ and $\sigma = 0.6(1)$ for the strongly screened vortex glass model. Note that in $d = 3$ all the critical exponents of the NWP problem appear to be quite close to those that describe the strongly screened vortex glass model analyzed in Ref. [8]. As regards this, it appears to be tempting to conclude that in $d = 3$ both models are in the same universality class.

Acknowledgments

LA acknowledges a scholarship of the German academic exchange service DAAD within the "Research Internships in Science and Engineering" (RISE) program and the City College Fellowship program for further support. OM acknowledges financial support from the DFG (*Deutsche Forschungsgemeinschaft*) under grant HA3169/3-1. The simulations were performed at the HPC Cluster HERO, located at the University of Oldenburg (Germany) and funded by the DFG through its Major Instrumentation Programme (INST 184/108-1 FUGG) and the Ministry of Science and Culture (MWK) of the Lower Saxony State and at the GOLEM I cluster for scientific computing, also located at the University of

Oldenburg.

[1] K. Kremer, Z. Phys. B **45**, 149 (1981).
[2] M. Kardar and Y. C. Zhang, Phys. Rev. Lett. **58**, 2087 (1987).
[3] B. Derrida, Physica A **163**, 71 (1990).
[4] P. Grassberger, J. Phys. A **26**, 1023 (1993).
[5] R. Parshani, L. A. Braunstein, and S. Havlin, Phys. Rev. E **79**, 050102 (2009).
[6] A. K. Nguyen and A. Sudbø, Phys. Rev. B **57**, 3123 (1998).
[7] A. K. Nguyen and A. Sudbø, Phys. Rev. B **60**, 15307 (1999).
[8] F. O. Pfeiffer and H. Rieger, J. Phys.: Condens. Matter **14**, 2361 (2002).
[9] F. O. Pfeiffer and H. Rieger, Phys. Rev. **E 67**, 056113 (2003).
[10] K. Kajantie, M. Laine, T. Neuhaus, A. Rajantie, and K. Rummukainen, Phys. Lett. B **482**, 114 (2000), A summary of this article is available at papercore.org, see http://www.papercore.org/Kajantie2000.
[11] M. Camarda, F. Siringo, R. Pucci, A. Sudbø, and J. Hove, Phys. Rev. B **74**, 104507 (2006).
[12] N. D. Antunes and L. M. A. Bettencourt, Phys. Rev. Lett. **81** (1998).
[13] H. Hindmarsch and K. Strobl, Nucl. Phys. **B 437**, 471 (1995).
[14] K. Strobl and M. Hindmarsh, Phys. Rev. E **55**, 1120 (1997).
[15] M. Cieplak, A. Maritan, and J. R. Banavar, Phys. Rev. Lett. **72**, 2320 (1994).
[16] O. Melchert and A. K. Hartmann, Phys. Rev. B **76**, 174411 (2007).
[17] K. Schwarz, A. Karrenbauer, G. Schehr, and H. Rieger, J. Stat. Mech. **2009**, P08022 (2009).
[18] C. Papadimitriou and K. Steiglitz, *Combinatorial Optimization – Algorithms and Complexity* (Dover Publications Inc., Mineola, NY, 1998).
[19] D. Stauffer, Phys. Rep. **54**, 1 (1979).
[20] D. Stauffer and A. Aharony, *Introduction to Percolation Theory* (Taylor and Francis, London, 1994).
[21] A. M. J. Schakel, Phys. Rev. E **63**, 026115 (2001).
[22] O. Melchert and A. K. Hartmann, New. J. Phys. **10**, 043039 (2008).
[23] O. Melchert, L. Apolo, and A. K. Hartmann, Phys. Rev. E **81**, 051108 (2010).
[24] L. Apolo, O. Melchert, and A. K. Hartmann, Phys. Rev. E **79**, 031103 (2009).
[25] *Papercore* is a free and open access database for summaries of scientific (currently mainly physics) papers., URL `http://www.papercore.org/`.
[26] R. K. Ahuja, T. L. Magnanti, and J. B. Orlin, *Network Flows: Theory, Algorithms, and Applications* (Prentice Hall, 1993).
[27] W. Cook and A. Rohe, INFORMS J. Computing **11**, 138 (1999).
[28] A. K. Hartmann and H. Rieger, *Optimization Algorithms in Physics* (Wiley-VCH, Weinheim, 2001).
[29] O. Melchert, *PhD thesis* (not published, 2009).
[30] A. K. Hartmann, *Practical Guide to Computer Simulations* (World Scientific, Singapore, 2009).
[31] For the calculation of minimum-weighted perfect matchings we use Cook and Rohes blossom4 extension to the Concorde library., URL `http://www2.isye.gatech.edu/~wcook/blossom4/`.